JGR Atmospheres

RESEARCH ARTICLE
10.1029/2021JD036204

Impacts of Suppressing Excessive Light Rain on Aerosol Radiative Effects and Health Risks

Yong Wang[1], Wenwen Xia[1], Guang J. Zhang[2], Bin Wang[1,3,4], and Guangxing Lin[5]

[1]Department of Earth System Science, Ministry of Education Key Laboratory for Earth System Modeling, Institute for Global Change Studies, Tsinghua University, Beijing, China, [2]Scripps Institution of Oceanography, La Jolla, CA, USA, [3]State Key Laboratory of Numerical Modelling for Atmospheric Sciences and Geophysical Fluid Dynamics, Institute of Atmospheric Physics, Chinese Academy of Sciences, Beijing, China, [4]College of Earth and Planetary Sciences, University of Chinese Academy of Sciences, Beijing, China, [5]International Center for Climate and Environment Sciences, Institute of Atmospheric Physics, Chinese Academy of Sciences, Beijing, China

Key Points:

- Suppression of light rain increases the total radiative effect of aerosols by −1.4 W/m^2, even larger than aerosol anthropogenic effects
- Elevated air pollution increases the health risks, with estimated global premature mortality increased by 300,000 deaths per year
- Reduced excessive light rain by suppressing too frequent convection has little effect on anthropogenic aerosol forcing

Correspondence to:
G. J. Zhang,
gzhang@ucsd.edu

Citation:
Wang, Y., Xia, W., Zhang, G. J., Wang, B., & Lin, G. (2022). Impacts of suppressing excessive light rain on aerosol radiative effects and health risks. *Journal of Geophysical Research: Atmospheres*, *127*, e2021JD036204. https://doi.org/10.1029/2021JD036204

Received 13 NOV 2021
Accepted 18 APR 2022

Abstract Global climate models (GCMs) have been used widely to study radiative forcing and health risks of aerosols. A recent study using two GCMs found that light rain plays a dominant role in controlling aerosol loading. However, "too much light rain and too little heavy rain" is a longstanding bias in GCMs. It is unclear how much light rain affects aerosol-cloud-radiation interactions and health risks from air pollution. Here we show that, with the correction of the rainfall intensity spectrum in the National Center for Atmospheric Research Community Atmosphere Model version 5.3 by introducing a stochastic deep convection scheme, the reduced frequency of light rain (1–20 mm d^{-1}) results in changes of aerosol direct radiative effects (DRE) of up to −0.5 ± 0.03 W/m^2 and aerosol cloud radiative effects (CRE) of up to −0.9 ± 0.03 W/m^2. The total (CRE + DRE) radiative effects of light rain-mediated aerosol changes exceed the present-day anthropogenic forcing of aerosols relative to preindustrial levels from the Coupled Model Intercomparison Project (CMIP5&6) models. However, the correction of the rainfall intensity spectrum has little effect on anthropogenic aerosol forcing (defined as the radiative perturbation due to changes in aerosol concentrations between the industrial era and preindustrial levels). Due to increased exposure to fine particulates ($PM_{2.5}$), the estimated global total premature mortality is much higher than previously estimated, by 300,000 ± 60,000 deaths per year, and is more severe in populous regions such as India and China. The findings in this study highlight the need to understand uncertainties in radiative effects and health risks of aerosols due to simulation biases of precipitation in GCMs.

Plain Language Summary All global climate models have a problem of "too much light rain and too little heavy rain". Climatologically, light rain plays a disproportionate role in controlling the aerosol loading and thus can affect aerosol radiative effects and health risks. Here, we show that correcting this issue in a global climate model leads to substantial increases of the radiative effects and health risks of aerosols. The resulting change of the radiative effects is even larger than present-day anthropogenic forcing of aerosols relative to preindustrial levels. The global total premature mortality due to elevated air pollution level is increased significantly.

1. Introduction

Aerosols modulate Earth's energy balance both directly and indirectly. Directly they scatter or absorb solar radiation, and indirectly they alter cloud micro- and macro-physical properties by serving as cloud ice and condensation nuclei (Boucher et al., 2013; Y. Wang et al., 2014). The effective radiative forcing (ERF, defined as Earth's energy imbalance to a radiative perturbation) (Forster et al., 2016; Myhre et al., 2013) from aerosol-radiation-interaction (ERFari) and aerosol-cloud interaction (ERFaci) due to changes in aerosol concentrations in the industrial era (present-day, PD) relative to preindustrial (PI) levels has been quantified by global climate models (GCMs). In the fifth phase of the Coupled Model Intercomparison Project (CMIP5), the total (shortwave + longwave) ERF due to anthropogenic aerosols (ERFari + aci) was estimated to be −1.17 ± 0.30 W/m^2, with ERFari of −0.25 ± 0.22 W/m^2 and ERFaci of −0.92 ± 0.34 W/m^2, respectively (Zelinka et al., 2014). Its updated value from CMIP6 models is −1.04 ± 0.20 W/m^2, with −0.23 ± 0.19 W/m^2 from ERFari and −0.81 ± 0.30 W/m^2 from ERFaci (Smith et al., 2020). Observationally, Chung et al. (2005) estimated ERFari to be −0.35 W m^{-2} with a range of −0.6 to −0.1 W m^{-2} from satellite and ground-based observations. Using satellite-based estimation, Jia

et al. (2021) reported the ERFaci to be between −1.09 and −0.59 W m^{-2}. With constraints from such observations, the combined total ERF due to anthropogenic aerosols is assessed to be between −1.6 and −0.6 W m^{-2} at the 16%–84% confidence level (Bellouin et al., 2020). Besides the radiative effects, air pollution from aerosols are harmful to human health. Long-term exposure to $PM_{2.5}$ (particulate matters with diameters less than 2.5 μm) in the air can increase the risks of respiratory and cardiovascular diseases, and premature mortality (Chowdhury et al., 2018; Park et al., 2020; Silva et al., 2017).

Atmospheric aerosols are affected by emission, secondary production, transport, dry and wet deposition. Among them, the wet removal by precipitation is a major sink of aerosols in the atmosphere, especially submicron particles (Rasch et al., 2000). However, "too much light rain and too little heavy rain" is a common precipitation bias in all current GCMs (Na et al., 2020). Efforts have been made to alleviate this bias from parametrizations of cloud microphysics (Golaz et al., 2011; Jing & Suzuki, 2018) and convection (Y. Wang et al., 2016). Golaz et al. (2011) modified the threshold of droplet effective radius for the onset of rainfall in the Geophysical Fluid Dynamics Laboratory Climate Model version 3 and Jing and Suzuki (2018) replaced the default warm-rain scheme (Berry, 1968) with the Khairoutdinov and Kogan (2000) scheme in the Model for Interdisciplinary Research on Climate version 5.2. Their modifications, to some extent, mitigated the problem of too frequent warm rain in GCMs. However, suppressing the excessive occurrence of light rain from cloud microphysics parameterizations is not as effective as from convection schemes (Y. Wang, Xia, et al., 2021) because too frequent convection is the main factor (D. Chen et al., 2021). Despite this, Golaz et al. (2011) and Jing and Suzuki (2018) noted that the perturbed radiative effects of aerosols by the altered light rain frequency are substantial.

Y. Wang, Xia, et al. (2021) showed that, when light rain was suppressed by improving convection parameterization (Y. Wang, Zhang, et al., 2021; Y. Wang et al., 2016, 2017), it had a profound impact on the atmospheric aerosol concentration. The aerosol optical depth (AOD) increased at the global scale, especially in the rain belts over the tropics and subtropics, by as much as 0.3. This finding raises two important questions. How much does changing light rain statistics perturb aerosol-cloud-radiation interactions? How much does the increased air pollution level elevate the health risks?

To answer these questions, we analyze four simulations from the National Center for Atmospheric Research (NCAR) Community Atmosphere Model version 5.3 (CAM5.3). Two are from the standard CAM5.3 model with and without prescribed climatological aerosols and the other two have the same setups except including a stochastic convection scheme that has mitigated the "too much light rain and too little heavy rain" problem (Plant & Craig, 2008; Y. Wang et al., 2016). We also conduct two additional experiments with and without the stochastic convection using the PI aerosol and aerosol precursor emissions (see Section 2.2 below).

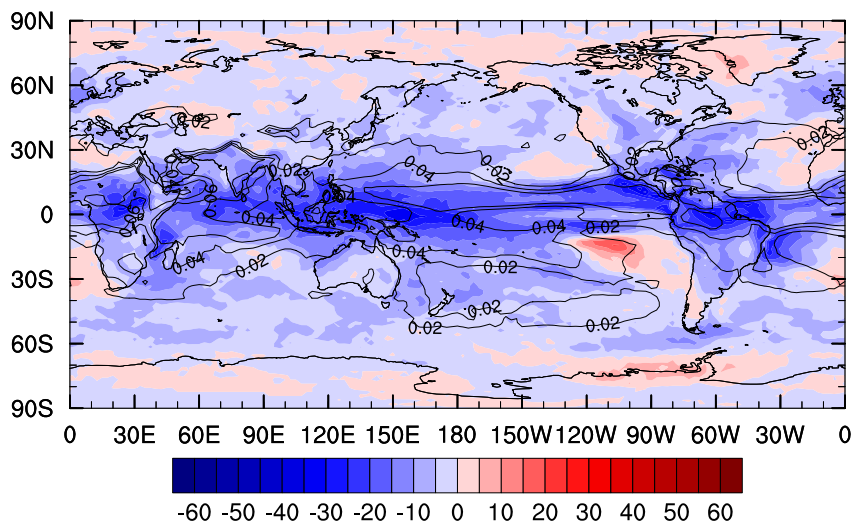

Figure 1. Global distribution of light-rain frequency ($1 < P < 20$ mm d^{-1}) differences (shading) between the Community Atmosphere Model version 5 (CAM5) and STOC simulations (STOC minus CAM5). Contours (with intervals of 0.02) represent the increase of aerosol optical depth after suppressing excessive light rain.

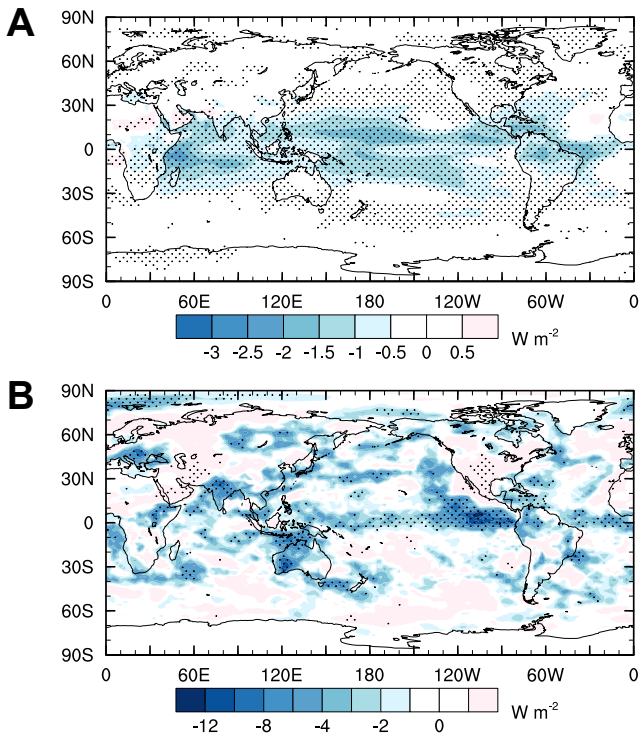

Figure 2. Global distributions of changes of aerosol (a) direct radiative effects and (b) cloud radiative effects from Community Atmosphere Model version 5 to STOC simulations. Areas exceeding 95% *t*-test confidence level are stippled.

The manuscript is organized as follows. The analysis methodology, including CAM5, experiments, observations, aerosol DRE (direct radiative effects) and CRE (cloud radiative effects) calculations, and an integrated exposure-response (IER) model, is presented in Section 2. Results on elevated radiative effects and health risks of aerosols after suppressing excessive light rain are shown in Section 3. Section 4 summarizes the findings of this work.

2. Methodology

2.1. CAM5

CAM5.3 is the atmospheric component of the NCAR Community Earth System Model version 1 (CESM1). It has a horizontal resolution of 1.9° × 2.5° and a vertical resolution of 30 levels from the surface to 3.6 hPa, with a finite volume dynamical core. For the physics parameterization suite, deep convection is parameterized following Zhang and McFarlane (1995) (i.e., the Zhang-McFarlane [ZM] scheme) with modifications by Neale et al. (2008) to use dilute convective available potential energy in the convective closure. The shallow convection is parameterized using the Park and Bretherton (2009) scheme. The stratiform cloud microphysics parametrization uses the Morrison and Gettelman (2008) scheme. The aerosol properties and processes are treated using the modal aerosol module (MAM) of Liu et al. (2012). The size distributions of aerosols are represented by three lognormal modes (MAM3): Aitken, accumulation and coarse modes. The mass and number concentrations of different aerosols in each mode are predicted. The total $PM_{2.5}$ mass concentrations are the sum of the total mass in the Aitken and accumulation modes and some of the coarse mode. To derive the contribution from the coarse mode, the integrated mass concentration from the log-normal spectrum up to 2.5 μm is calculated. In addition to convection, clouds and aerosol parameterizations, boundary layer turbulence is parameterized using Bretherton and Park (2009) moist turbulence scheme. The radiative transfer is parameterized using the Rapid Radiative Transfer Model of Iacono et al. (2008).

The most relevant process to this study is wet scavenging of aerosols by precipitation. The aerosol wet scavenging subroutine in MAM3 treats in- and below-cloud removal (Liu et al., 2012). The in-cloud wet scavenging removes cloud-borne (i.e., activated) aerosol particles and the below-cloud scavenging removes interstitial aerosol particles by raindrops through impaction and Brownian diffusion. For in-cloud wet scavenging in stratiform clouds, the production rates of large-scale precipitation (kg kg^{-1} s^{-1}) and mass mixing ratios of cloud water (kg kg^{-1}) are applied to derive cloud-water first-order loss rates (s^{-1}). The first-order loss rates of cloud water are multiplied by "wet removal adjustment factors" to calculate the first-order loss rates of aerosols, which are applied to cloud-borne aerosols in the non-ice clouds for a given grid cell. The in-cloud scavenging in stratiform clouds

Table 1
Global Means of Aerosol Direct Radiative Effects (DRE; $F - F_{clean}$) and Cloud Radiative Effects (CRE; $F_{clean} - F_{clean,clear}$) in Each Simulation[a]

	DRE			CRE[b]		
	SW	LW	SW + LW	SW	LW	SW + LW
CAM5 (A)	−1.5 ± 0.01	0.2 ± 0.00	−1.3 ± 0.01	−53.8 ± 0.23	24.2 ± 0.08	−29.6 ± 0.20
STOC (B)	−2.0 ± 0.02	0.3 ± 0.00	−1.8 ± 0.02	−50.6 ± 0.15	22.2 ± 0.06	−28.4 ± 0.21
CAM5-PM (C)	−1.4 ± 0.00	0.2 ± 0.00	−1.2 ± 0.00	−53.9 ± 0.22	24.2 ± 0.09	−29.7 ± 0.23
STOC-PM (D)	−1.4 ± 0.01	0.2 ± 0.00	−1.2 ± 0.01	−50.0 ± 0.18	22.4 ± 0.06	−27.5 ± 0.16

[a]SW for shortwave and LW for longwave. [b]Due to the correction of the rainfall intensity spectrum, the change of aerosol CRE is −0.9 ± 0.23 W/m^2 derived from B minus D.

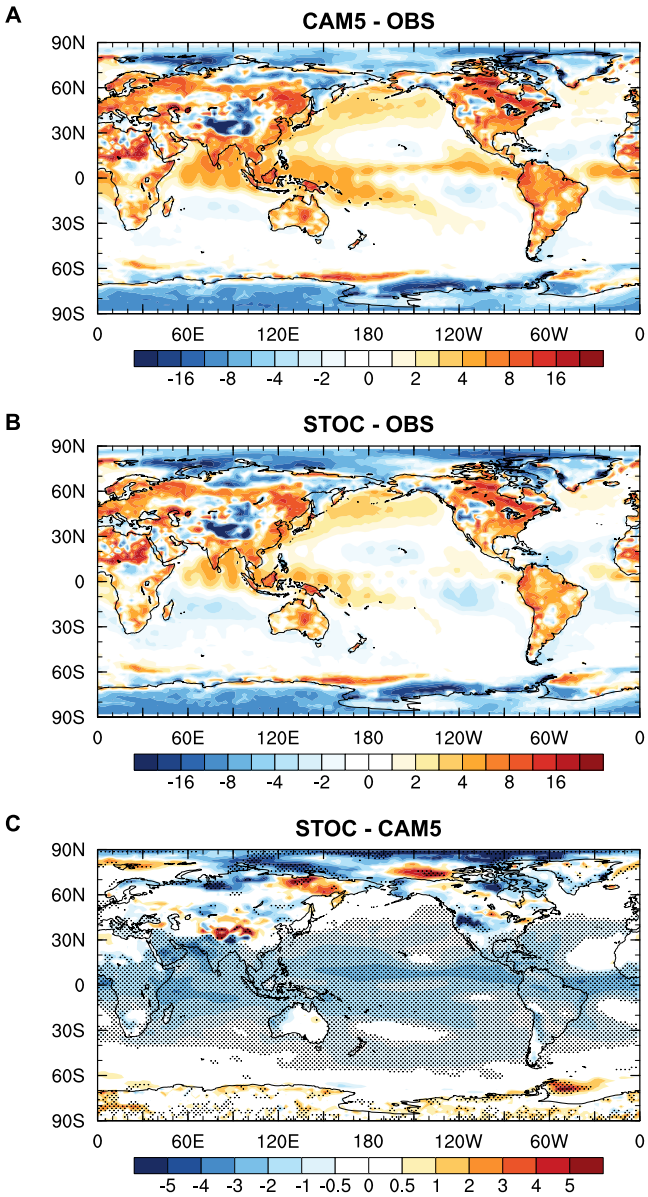

Figure 3. Global distributions of clear-sky top-of-atmosphere net radiation biases in the (a) Community Atmosphere Model version 5 (CAM5) and (b) STOC runs compared to the Clouds and the Earth's Radiant Energy System satellite observations and (c) differences between the CAM5 and STOC runs.

Table 2
Key Parameters for the Integrated Exposure-Response Model

Mortality	α	γ	δ	C_0
COPD	0.565	0.019	0.861	5.8
LC	0.841	0.014	0.915	5.8
IHD	1.043	0.104	0.684	5.8
Stroke	1.579	0.013	1.235	5.8

only affects the stratiform-cloud-borne aerosol particles not interacting with convective clouds. The adjustment factor for the stratiform in-cloud scavenging is currently set to 1.0. Note that the interstitial aerosol particles are not affected by the stratiform in-cloud wet scavenging. In-cloud scavenging is not considered in stratiform ice clouds either.

The treatment of in-cloud wet scavenging for convective clouds including both deep and shallow convection uses in-cloud condensate mixing ratio, cloud fraction and grid mean convective rainfall production (derived from shallow and deep convection parameterizations) to obtain cloud-water first-order loss rates (s^{-1}). Different from the stratiform cloud-borne aerosol particles, the convective cloud-borne aerosols are not explicitly treated, which are equal to the product (lumped interstitial aerosols) × (convective-cloud activation fraction). Thus, it only influences the grid mean interstitial aerosols. The prescribed parameter of convective cloud activation varies with aerosol species and mode. For example, 0.8 and 0.4 are used for sea salt and dust aerosols, respectively, in the coarse mode and a weighted average is used for the coarse mode sulfate and number. Similarly, the first-order loss rates of cloud water are multiplied by "wet removal adjustment factors" to calculate the first-order loss rates of aerosols, which are applied to derive convective cloud-borne aerosol particles. Here, the wet removal adjustment factor of 0.4 is applied to convective clouds to suppress wet removal by convection.

For below-cloud wet scavenging of interstitial aerosols, the first-order scavenging rate is equal to precipitation rate multiplied by a scavenging coefficient. The large-scale precipitation rate is used for stratiform cloud scavenging and the convective precipitation rate is used for convective cloud scavenging. The scavenging coefficient is derived based on Y. Wang et al. (2010), in which the collection rate of a single aerosol particle by a single raindrop is integrated over their size distributions, at a rain rate of 1 mm hr^{-1}. A Marshall-Palmer size distribution of raindrops and collection efficiencies from Slinn (1984) are assumed. The scavenging coefficients differ greatly for different aerosol particle sizes, with the lowest values for aerosols in the accumulation mode. No wet removal of stratiform-cloud-borne aerosols is treated below clouds.

2.2. Experiments

Using the NCAR CAM5, we performed four Atmospheric Model Intercomparison Project type simulations with the aerosol scenario of PD aerosol emissions and two with PI aerosol emissions. For each group with the same aerosol and aerosol precursor emissions, there are two experiments with the default ZM deep convection scheme (CAM5 and CAM5-PI) and the stochastic deep convection parameterization (STOC and STOC-PI) respectively, which are forced by observed seasonally varying PD (averaged over 1982–2001) climatological sea surface temperatures and sea ice extent. With these experiments, the change of ERFaci between CAM5 and STOC can be derived. In addition to the above four simulations, we conducted two more simulations, CAM5-PM and STOC-PM, which are the same as the CAM5 and STOC runs, respectively, but are subjected to the prescribed climatological aerosols from the CAM5 run. This allows us to quantify the aerosol CRE by excluding the impacts of liquid water path (LWP) and cloud fraction changes caused by altered meteorological conditions after the implementation of the stochastic parameterization. All simulations are run for 6 years and the last 5 years of data are used for analysis.

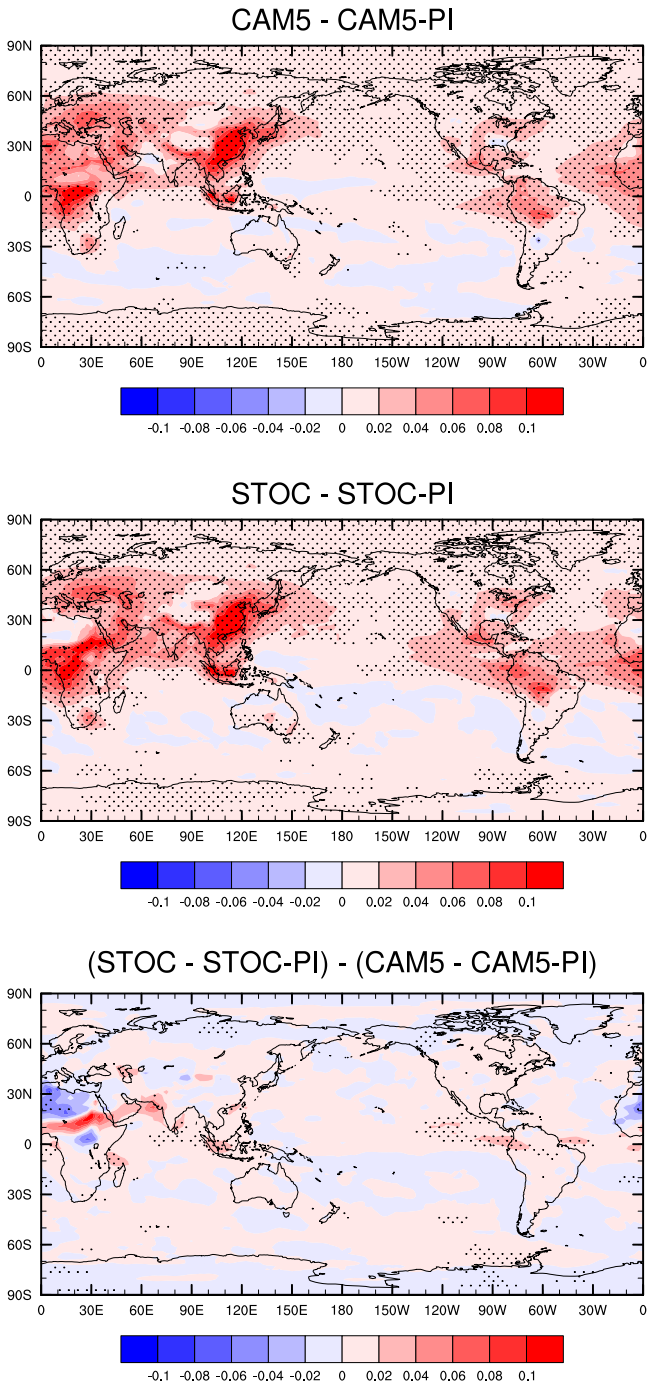

Figure 4. Differences of aerosol optical depth between present-day and preindustrial for Community Atmosphere Model version 5 (CAM5) and STOC, and their changes from CAM5 to STOC.

2.3. Observations

The clear-sky top-of-atmosphere (TOA) net radiation is strongly affected by atmospheric aerosols. To verify whether its simulation can be improved as the AOD increases after suppressing the too much light rain, the Clouds and the Earth's Radiant Energy System level-3b EBAF observations with a resolution of 1° × 1° (Kato et al., 2018) are used. In addition, the near-surface $PM_{2.5}$ concentrations over India and China are evaluated by in situ observations from the World Air Quality Index Project (https://aqicn.org/data-platform/covid19).

2.4. Aerosol DRE and CRE Calculations

Following Ghan (2013), the change of aerosol DRE is estimated as $\Delta(F - F_{clean})$, where Δ, depending on the application, can be the difference between the STOC and CAM5 runs or between the PD and PI emissions, F is the TOA net radiative flux (including both shortwave and longwave components) and F_{clean} is a diagnostic TOA net radiative flux, but neglecting scattering and absorption of radiation by individual aerosol species. The aerosol CRE is calculated as $\Delta(F_{clean} - F_{clean,clear})$, where $F_{clean,clear}$ is a diagnostic TOA net radiative flux neglecting the absorption and scattering of radiation by both aerosols and clouds. Note that these calculations are different from the traditionally defined radiative effects of aerosols because we are also comparing experiments with different rainfall intensity spectra, as opposed to different emissions only. Three factors affect the radiative effects of aerosol-cloud interaction: LWP, cloud droplet radius and cloud cover (Goren & Rosenfeld, 2014). For a given LWP, increased aerosols can enhance the reflection of solar radiation (a cooling effect) because more but smaller cloud droplets can form as a result of more aerosols in a cloud (Twomey, 1977). Meanwhile, the increased concentration of CCN associated with increased aerosols can reduce the rainfall efficiency, resulting in an increase of the LWP and the increased cloud cover and cloud lifetime (Albrecht, 1989). LWP and cloud cover can also be regulated by meteorological conditions (i.e., changes not caused by the aerosol changes) which are altered after the stochastic convection scheme is used. There are large decreases of cloud cover over the tropics and increases (decreases) in LWP over oceans (land) (Y. Wang & Zhang, 2016). The altered LWP and cloud cover not related to aerosol changes could contaminate the estimates of aerosol CRE changes. To estimate the impact of non-aerosol-induced cloud fraction and LWP changes on the aerosol CRE changes, two additional simulations, as mentioned before, are conducted. The global mean aerosol DRE and CRE in each simulation are summarized in Table 1. For CAM5-PM, which uses the prescribed climatological aerosols from CAM5, the SW and LW CRE are the same as those in CAM5, as expected. As such, given STOC-PM with the prescribed aerosol concentrations as in CAM5 and STOC with the interactive aerosol concentrations, we can directly take the difference between STOC and STOC-PM (STOC-PM minus STOC) to obtain perturbed aerosol CRE due to aerosol changes only. Similarly, the ERFaci can be diagnosed also using the same approach of $\Delta(F_{clean} - F_{clean,clear})$. Here Δ represents the difference between the PD and PI simulations (PD-PI) with/without the correction of the rainfall intensity spectrum. Thus, the ERFaci differences demonstrate the variations in radiation sensitivity to perturbations of aerosols due to rainfall spectrum correction, which is important for projections of future climate.

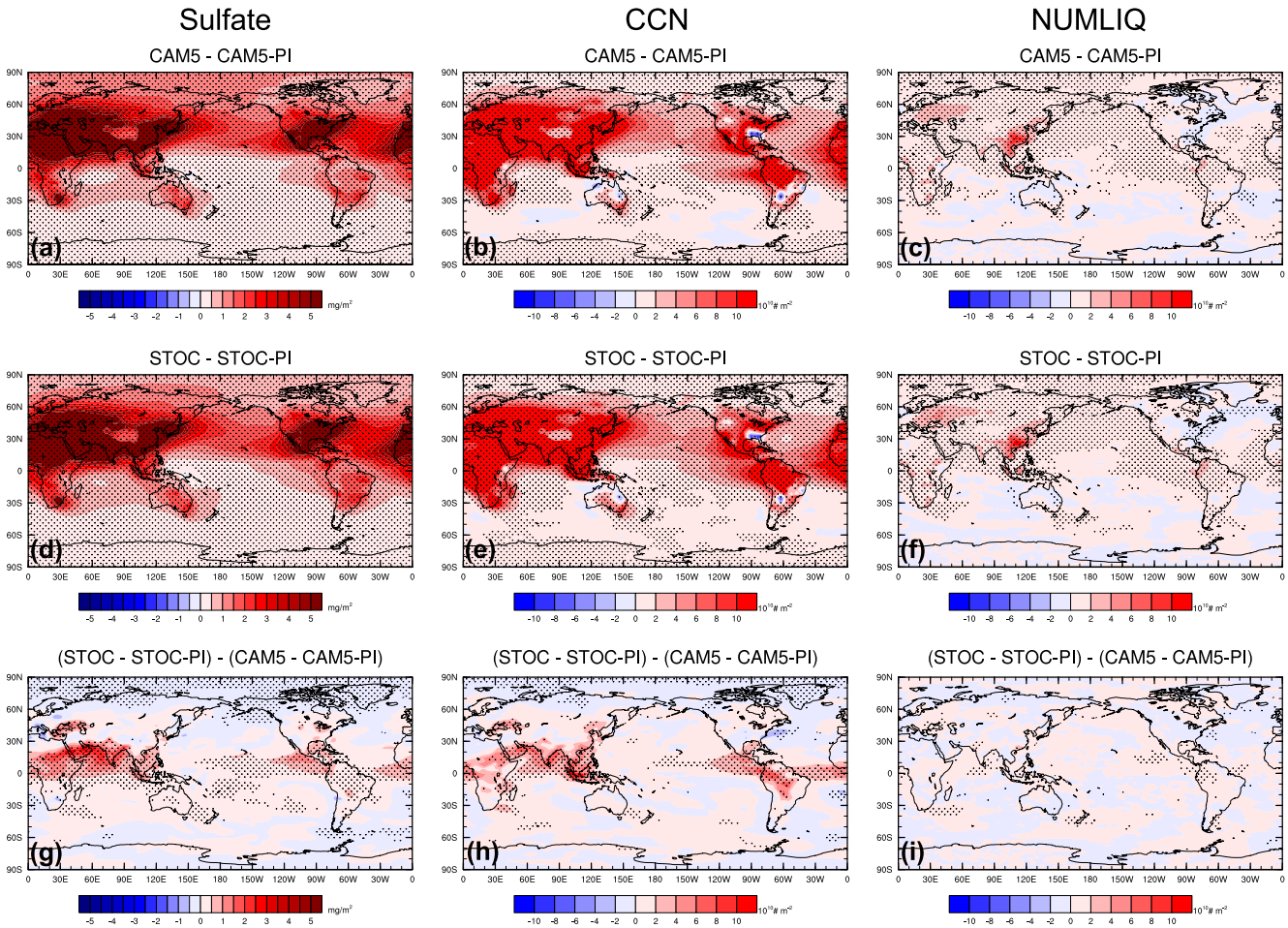

Figure 5. Same as Figure 4, but for (a, d and g) sulfate burden (mg/m^2), (b, e and h) vertically integrated CCN (10^{10}#/m^2) and (c, f and i) vertically integrated cloud droplet number concentrations (NUMLIQ) (10^{10}#/m^2).

2.5. Integrated Exposure-Response Model

The IER model developed by Burnett et al. (2014) is applied to calculate the $PM_{2.5}$-related premature deaths. This model has been used widely to quantify health effects of air pollution (Apte et al., 2015; Burnett et al., 2014; Zhao et al., 2019). Exposure to high $PM_{2.5}$ concentrations penetrating deep into lung passageways can lead to a variety of health issues. Here we focus on four main diseases directly related to ambient $PM_{2.5}$ exposure: stroke, ischemic heart disease (IHD), lung cancer (LC), and chronic obstructive pulmonary disease (COPD). The $PM_{2.5}$ concentrations simulated by each simulation are taken as the exposure input of the IER model.

Table 3
Global Means of Changes in Aerosol Direct Radiative Effects (DRE) and Cloud Radiative Effects (CRE), and Global Means of ERFaci With/Without the Correction of the Rainfall Intensity Spectrum and the Total $PM_{2.5}$-Related Premature Mortality in the Specific Simulation

	ΔDRE (W/m^2)	ΔCRE (W/m^2)	Simulations	Total premature mortality (1,000 deaths per year)
STOC – CAM5	−0.5 ± 0.03	−0.9 ± 0.23	CAM5	3,849.1
Aerosol emissions (PD-PI)[a]	ERFaci			
CAM5—CAM5-PI	−1.53 ± 0.2		STOC	4,164.4
STOC—STOC-PI	−1.60 ± 0.2			

[a]PD is for present-day aerosol emissions and PI represents preindustrial emissions respectively.

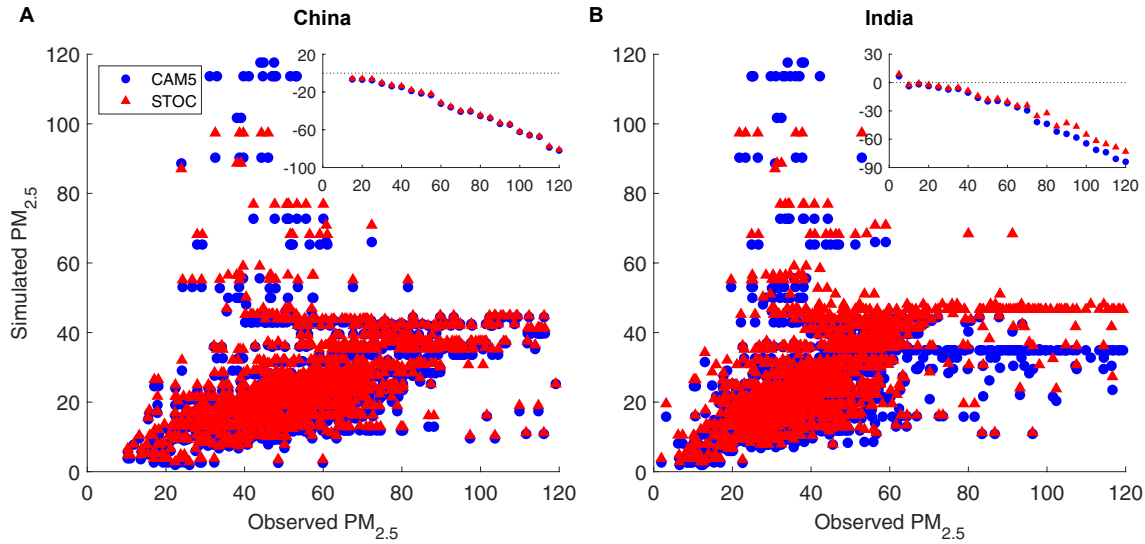

Figure 6. Observed and simulated surface $PM_{2.5}$ concentrations (μg m^{-3}) over (a) China and (b) India. The inset frame represents the average biases of modeled $PM_{2.5}$ concentrations in each binned observed $PM_{2.5}$ concentrations with an interval of 5 μg m^{-3}.

The relative risk (RR) for each disease estimated by the IER model is calculated as:

$$\mathrm{RR}(C) = \begin{cases} 1 + \alpha \left[1 - \exp\left(-\gamma(C - C_0)^{\delta}\right)\right], & \text{for } C > C_0 \\ 1, & \text{for } C \le C_0 \end{cases} \quad (1)$$

where C is the simulated annual mean $PM_{2.5}$ mass concentration, C_0 is the counterfactual concentration below which there is no excess health damage and is set to 5.8 μg m^{-3} as in Chowdhury and Dey (2016), and α, γ and δ are parameters determining the shape of the concentration-response curve. Their values used in this work, which is also used in S. Chen et al. (2019), are listed in Table 2. In Burnett et al. (2014), there are a thousand estimates of (α, γ, δ) and C_0 has a range of 5.8–8.8 μg/m^3. To evaluate the uncertainty range of the resultant mortality differences between the CAM5 and STOC runs, we use the parameters to conduct 1,000 sets of Monte Carlo simulations and a standard deviation of ~60,000 deaths per year is derived.

The attributable fraction (AF) of deaths due to $PM_{2.5}$ pollution for a given disease is then estimated from RR by:

$$\mathrm{AF} = \frac{\mathrm{RR} - 1}{\mathrm{RR}} \quad (2)$$

The corresponding premature mortality is further quantified in the following form:

$$M = \mathrm{AF} \times B \times P \quad (3)$$

where B is the baseline mortality rate for a given cause, P is the population density obtained from the Gridded Population of the World data set version 3 (http://sedac.ciesin.columbia.edu/gpw) which provides the global population density with a 0.5° × 0.5° resolution every 5 years from 1990 to 2010. The baseline mortality data are available from Global Burden of Disease Study 2017 (Roth et al., 2018).

3. Results

3.1. Radiative Effects

The use of stochastic convection parameterization greatly suppresses the occurrence of light rain in the range from 1 to 20 mm d^{-1} (Figure 1). Consequently, the AOD is enhanced globally, particularly over the tropics and subtropics, with the pattern of change highly resembling that of the light rain frequency. As a result of the light rain-induced increases of aerosols, the aerosol DRE is increased, giving an additional global annual mean cooling effect of −0.5 ± 0.03 W/m^2 (mean ± one standard deviation) (Table 3) from shortwave radiation change

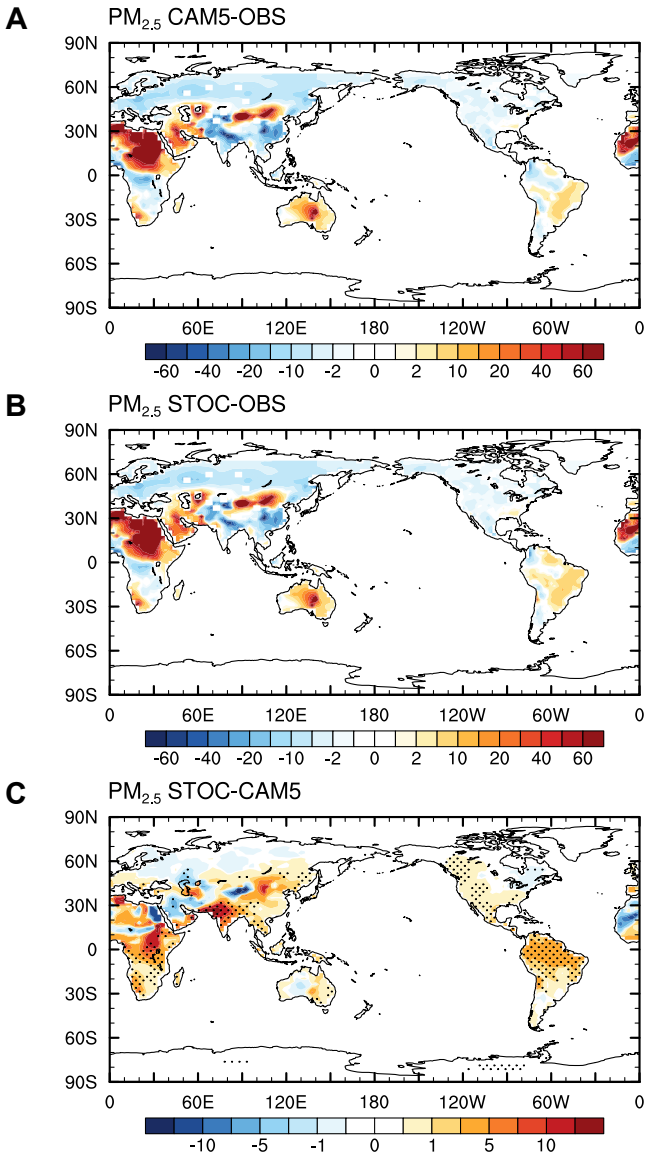

Figure 7. Global distributions of surface $PM_{2.5}$ concentration (μg m^{-3}) biases in the (a) Community Atmosphere Model version 5 (CAM5) and (b) STOC runs compared to the Socioeconomic Data and Applications Center (SEDAC) global $PM_{2.5}$ product and (c) differences between the STOC and CAM5 simulations. The annual mean $PM_{2.5}$ concentrations from SEDAC are averaged over 1998–2002.

(Table 1). The most significant aerosol DRE changes are over the tropics and subtropics, by as much as −3.0 W/m^2 (Figure 2a). After eliminating the impact of changes in cloud fraction and LWP from altered meteorological conditions on changes of aerosol CRE, the change of the global annual mean CRE of all aerosols (both natural and anthropogenic) due to changes of the rainfall intensity spectrum is -0.9 ± 0.23 W/m^2 (Table 3). The largest cooling effect from CRE is also over the tropics and subtropics (Figure 2b). Note that the inclusion of the stochastic deep convection scheme has led to an improved longwave and shortwave cloud radiative forcing (Y. Wang & Zhang, 2016) and clear-sky TOA net radiation (Figure 3). The positive biases broadly distributed over the global land surfaces in the CAM5 simulation (Figure 3a), except for those covered by the vast ice sheet (e.g., the Tibet Plateau, Arctic and Antarctica) where negative biases exist, are alleviated in the STOC simulation (Figure 3b). The largest improvements are noted over oceans especially over the Western Pacific, the Intertropical Convergence Zone and the Indian Ocean, and those continents with heavy aerosol loadings such as South Asia, Central Africa, Amazon, and the Middle East (Figure 3c). In East Asia, where there is also heavy aerosol loading, however, there are no obvious increases due to infrequent convection relative to that in the tropics and subtropics.

The increased aerosol loading from the reduced wet removal by less frequent light rain results in an aerosol DRE change that is twice as large as ERFari from anthropogenic aerosols. Meanwhile, the aerosol CRE change is comparable to ERFaci. These demonstrate that the aerosol radiative effects due to altered aerosol-cloud-radiation interactions by the reduction of light rain can be as large as or exceed the anthropogenic forcing of aerosols in the industrial era relative to PI levels. We should point out that with the stochastic scheme, the occurrence frequency of light rain is still overestimated compared to observations (Y. Wang et al., 2016; Y. Wang, Xia, et al., 2021). Thus, if the bias of the excessive light rain is entirely eliminated, the total radiative effect from aerosol-cloud-radiation interactions could be larger than −1.4 W/m^2 (i.e., $-0.5 + -0.9$ W/m^2) in magnitude.

These changes may have implications on the accuracy of the estimate of aerosol effects on future climate change. Despite the large DRE and CRE changes, the correction of the rainfall intensity spectrum has little effect on the ERFari and ERFaci, which are -0.02 ± 0.01 and -1.60 ± 0.2 W/m^2 for the simulation with reduced light rain and -0.01 ± 0.02 and -1.53 ± 0.2 W/m^2 for the default model simulation (Table 3), respectively. This is because the differences of AOD, aerosol composition burdens (e.g., sulfate), cloud condensation nuclei concentrations and cloud droplet number concentrations between the PD and PI aerosol and aerosol precursor emission simulations (Figures 4 and 5) are comparable in the simulations with and without the corrected rainfall intensity spectrum. The reason for this is that most of convection occurs in the tropics, particularly over tropical oceans, whereas anthropogenic aerosols are mainly concentrated in midlatitude land, where convection occurs much less frequently. As a result, the wet removal of anthropogenic aerosols by convection is less efficient, leading to less difference of aerosol forcing when light rain frequency is altered.

We note that, unlike previous studies, which found amplified ERFaci when warm-rain microphysics was altered (Golaz et al., 2011; Jing & Suzuki, 2018), the correction of the rainfall intensity spectrum via improving parameterized convection is unlikely to affect the future climate projection as anthropogenic aerosol and aerosol precursor emissions change. One possible reason for the difference between the results from this study and the warm-rain microphysics work is that in Golaz et al. (2011) and Jing and Suzuki (2018), the warm-rain microphysics

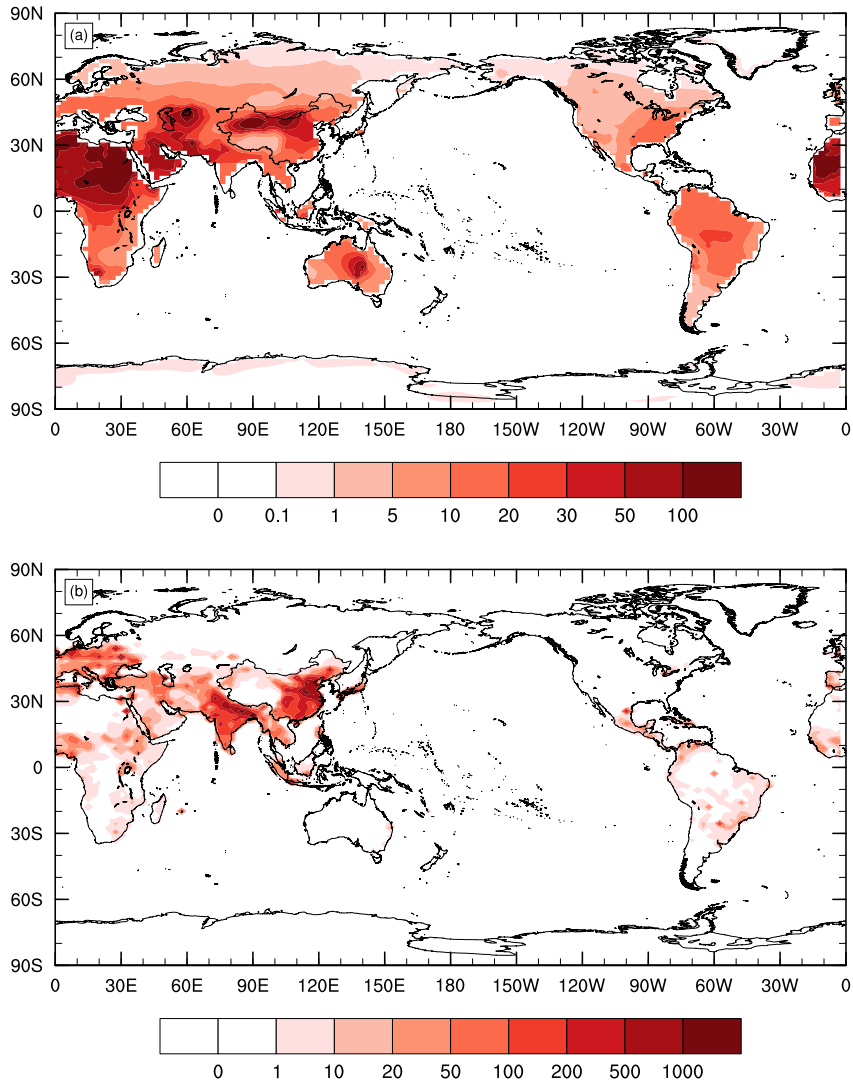

Figure 8. Global distributions of (a) $PM_{2.5}$ concentrations (μg m^{-3}) and (b) $PM_{2.5}$-related premature mortality (deaths per 1,000 km^2 per year) in the Community Atmosphere Model version 5 run.

schemes allow aerosols to modify cloud droplet radius, which can affect the subsequent warm rain. ERFaci is amplified in regions of stratiform clouds due to a positive feedback as noted in Jing and Suzuki (2018), that is, more aerosols lead to more cloud droplets with smaller radius, which suppress the warm rain. The suppressed warm rain further increases the aerosols due to the reduced wet removal. On the other hand, most convection schemes including the version of the ZM scheme used in this study do not include convective cloud microphysical processes, thus do not allow for aerosol modifications to cloud droplet radius and subsequent precipitation in convective clouds. Also, note that the increase of aerosols mainly occurs in the tropics and subtropics where convective clouds occur frequently (Figure 1). In contrast, in regions dominated by stratiform clouds such as the southeastern Pacific, there are no significant AOD increases. Therefore, ERFaci is not altered by modifying the convection scheme.

3.2. Health Risks

Among the aerosols, $PM_{2.5}$ is the most relevant to human health. Thus, we compare the simulated $PM_{2.5}$ concentrations with those from observations in India and China, where air pollution is the heaviest in the world (Figure 6). The simulated $PM_{2.5}$ is severely underestimated in both CAM5 and STOC, particularly at high pollution levels.

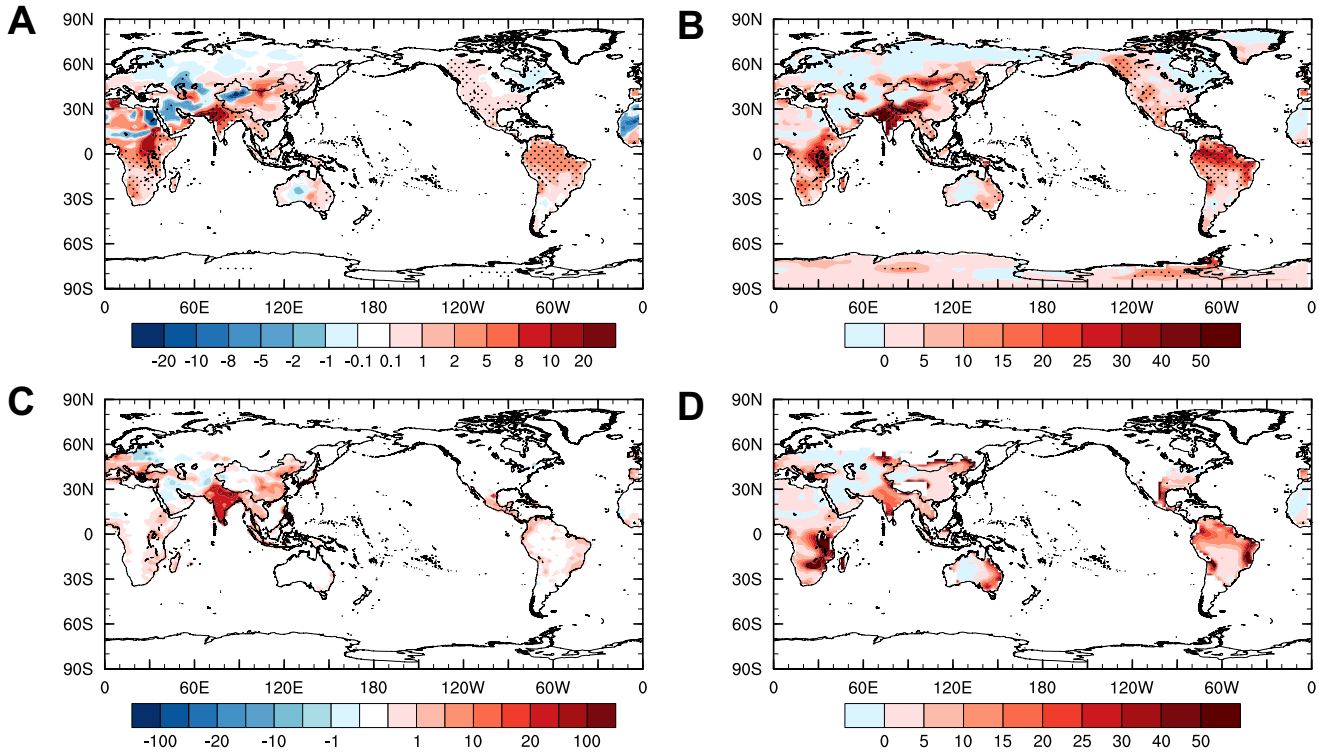

Figure 9. Global distributions of (a) absolute (μg m^{-3}) and (b) relative differences (%) of annual mean $PM_{2.5}$ concentrations between the STOC and Community Atmosphere Model version 5 simulations; panels (c and d) same as panels (a and b), but for $PM_{2.5}$-related premature mortality (deaths per 1,000 km^2 per year in panel (c) and % in panel (d)). Areas in panels (a and b) exceeding 95% *t*-test confidence level are stippled.

Nonetheless, the underestimation of $PM_{2.5}$ concentrations is alleviated to some extent in STOC relative to CAM5. In particular, over India, the improvement is more notable where the observed air pollution level is high as shown by the inset of Figure 6b. In comparison with the global $PM_{2.5}$ gridded product from SEDAC (Socioeconomic Data and Applications Center; Hammer et al., 2022; Figure 7), the underestimation of surface $PM_{2.5}$ concentrations over land (e.g., Europe and the United States) in CAM5, except for the arid and semi-arid regions where the problem of the overestimated dust burden is well known, is mitigated with the increases in $PM_{2.5}$ concentrations in STOC.

The elevated aerosol burden can increase human health risks. Using the IER model described in Section 2.5, we estimated the premature deaths related to ambient $PM_{2.5}$ concentrations. Figure 8 shows the $PM_{2.5}$ concentration over global land and its related premature deaths in the default CAM5 model simulation. There is high $PM_{2.5}$ concentration in most of the world, including Africa, Middle East, Asia, and central Australia. The $PM_{2.5}$-related premature deaths are mostly in India and China due to high population in these regions (Figure 8b).

The increased aerosol burden resulting from the light rain reduction has important health ramifications. Figure 9 shows the global distribution of absolute and relative changes of $PM_{2.5}$ mass concentration and related premature mortality from CAM5 to STOC simulations. The annual mean $PM_{2.5}$ mass concentration is increased almost everywhere over global land, particularly in south Asia and central and southern Africa. The increases are more than 5 μg m^{-3} over central India and up to 20 μg m^{-3} in northwestern India and Pakistan (Figure 9a). These changes represent more than 50% increase in $PM_{2.5}$ level (Figure 9b) in these densely populated regions where the pollution level is already dangerously high (Figure 8a) except in arid and semi-arid regions where pollution is dominated by natural dust of larger sizes. Central and southern Africa, western North America, and South America also experience 20%–40% increases in $PM_{2.5}$ concentrations.

With increased $PM_{2.5}$ exposure, the estimated premature mortality is increased in many parts of the world, including East Asia, India, Europe (Figure 9c), where the pollution-related death toll is already high (Figure 8b), and Mexico. There are up to 100 more deaths per 1,000 km^2 annually in India, a nearly 50% increase from current

estimates. Although there are fewer deaths per 1,000 km^2 per year over southeastern Africa, the Caribbean, and South America, compared to India, the relative increase of premature mortality can be more than 50% (Figure 9d). Globally, the total number of deaths increases by more than 300,000 ± 60,000 per year, an increase of 8% in mortality rate.

4. Conclusions

With light-rain-induced increases of aerosols, the simulations of the clear-sky TOA net radiation and surface $PM_{2.5}$ concentrations are improved. The aerosol radiative effects and human health risks, which are underestimated in previous studies, are increased substantially. Aerosol DRE and CRE are increased by up to -0.5 ± 0.03 W/m^2 and up to -0.9 ± 0.03 W/m^2, respectively. These are as large as or exceed the anthropogenic forcing of aerosols in the industrial era relative to PI levels. The estimated global total premature mortality is increased by 300,000 ± 60,000 deaths per year and is more severe in populous regions such as India and China.

Many CMIP5&6 models underestimate aerosol burdens. Previous studies focused on revising the aerosol module to improve the simulation of aerosols. Some tuned the wet scavenging coefficients and others included missing sources for aerosol emissions (Xia et al., 2022). This study provides a very different but efficient way to mitigate the biased aerosol simulation by improving the simulated rainfall intensity spectrum. Atmospheric aerosol concentrations and associated aerosol radiative effects differ substantially in CMIP5&6 models, even with identical anthropogenic aerosol and aerosol precursor emissions (Smith et al., 2020; Zelinka et al., 2014). Although all current CMIP5&6 models overestimate the occurrence frequency of light rain, the magnitude and spatial pattern of overestimation among them differ significantly (Na et al., 2020). Therefore, this study implies that the difference of light-rain frequency in different CMIP5&6 models might be a main contributor to the uncertainties in the simulations of aerosols and associated aerosol radiative effects. As the climate warms, it is expected that there will be less light rain but more heavy rain. Thus, this work also has profound implications for understanding the role of light rain in the interactions of aerosols, cloud and climate and its impact on the aerosol health risks for future climate projections (Banks et al., 2022; Xu & Lamarque, 2018).

Data Availability Statement

The CESM1.2.1-CAM5.3 source code can be downloaded from the NCAR website http://www2.cesm.ucar.edu (CAM5.3, 2013). The stochastic convection code is available from an open repository Zenodo (https://doi.org/10.5281/zenodo.4543261; Stochastic Convection Scheme, 2021). The Clouds and the Earth's Radiant Energy System radiation data can be accessed online at https://ceres.larc.nasa.gov/ (CERES, 2018) and the observed $PM_{2.5}$ concentrations are from https://aqicn.org/data-platform/covid19 ($PM_{2.5}$, 2022). The CAM5 simulation output is provided in an open repository Zenodo (https://doi.org/10.5281/zenodo.4259554; CAM5 Simulations, 2022).

Acknowledgments

Y. Wang was supported by the National Key Research and Development Program of China Grant 2017YFA0604000 and the National Natural Science Foundation of China Grant 41975126. G. J. Zhang was supported by the US Department of Energy, Office of Science, Biological and Environmental Research Program (BER), under Award Number DE-SC0022064. The authors thank three anonymous reviewers for their constructive comments.

References

Albrecht, B. A. (1989). Aerosols, cloud microphysics, and fractional cloudiness. *Science*, *245*(4923), 1227–1230. https://doi.org/10.1126/science.245.4923.1227

Apte, J. S., Marshall, J. D., Cohen, A. J., & Brauer, M. (2015). Addressing global mortality from ambient $PM_{2.5}$. *Environmental Science & Technology*, *49*(13), 8057–8066. https://doi.org/10.1021/acs.est.5b01236

Banks, A., Kooperman, G. J., & Xu, Y. (2022). Meteorological influences on anthropogenic $PM_{2.5}$ in future climates: Species level analysis in the Community Earth System Model v2. *Earth's Future*, *10*(2), e2021EF002298. https://doi.org/10.1029/2021EF002298

Bellouin, N., Quaas, J., Gryspeerdt, E., Kinne, S., Stier, P., Watson-Parris, D., et al. (2020). Bounding global aerosol radiative forcing of climate change. *Reviews of Geophysics*, *58*(1), e2019RG000660. https://doi.org/10.1029/2019RG000660

Berry, E. X. (1968). Modification of the warm rain process. In *Paper presented at 1st National Conference on Weather Modification, April 28–May 1, American Meteorological Society, Albany, New York* (pp. 81–85).

Boucher, O., Randall, D., Artaxo, P., Bretherton, C., Feingold, G., Forster, P., et al. (2013). *Climate Change 2013: The Physical Science Basis. Contribution of Working Group I to the Fifth Assessment Report of the Intergovernmental Panel on Climate Change*. (In T. F. Stocker, D. Qin, G.-K. Plattner, M. Tignor, S. K. Allen, J. Doschung, et al., Eds.). Cambridge University Press.

Bretherton, C. S., & Park, S. (2009). A new moist turbulence parameterization in the Community Atmosphere Model. *Journal of Climate*, *22*(12), 3422–3448. https://doi.org/10.1175/2008jcli2556.1

Burnett, R. T., Pope, C. A., III, Ezzati, M., Olives, C., Lim, S. S., Mehta, S., et al. (2014). An integrated risk function for estimating the global burden of disease attributable to ambient fine particulate matter exposure. *Environmental Health Perspectives*, *122*, 397–403. https://doi.org/10.1289/ehp.1307049

CAM5.3. (2013). National Center for Atmospheric Research Community Atmosphere Model version 5.3 [Software]. Retrieved from http://www2.cesm.ucar.edu

CAM5 Simulations. (2022). CAM5 model output [Dataset]. Zenodo. https://doi.org/10.5281/zenodo.4259554

CERES. (2018). CERES radiation data [Dataset]. Retrieved from https://ceres.larc.nasa.gov/
Chen, D., Dai, A., & Hall, A. (2021). The convective-to-total precipitation ratio and the "drizzling" bias in climate models. *Journal of Geophysical Research: Atmospheres*, *126*(16), e2020JD034198. https://doi.org/10.1029/2020JD034198
Chen, S., Zhang, X., Lin, J., Huang, J., Zhao, D., Yuan, T., et al. (2019). Fugitive road dust $PM_{2.5}$ emissions and their potential health impacts. *Environmental Science & Technology*, *53*(14), 8455–8465. https://doi.org/10.1021/acs.est.9b00666
Chowdhury, S., & Dey, S. (2016). Cause-specific premature death from ambient $PM_{2.5}$ exposure in India: Estimate adjusted for baseline mortality. *Environment International*, *91*, 283–290. https://doi.org/10.1016/j.envint.2016.03.004
Chowdhury, S., Dey, S., & Smith, K. R. (2018). Ambient $PM_{2.5}$ exposure and expected premature mortality to 2100 in India under climate change scenarios. *Nature Communications*, *9*(1), 1–10. https://doi.org/10.1038/s41467-017-02755-y
Chung, C. E., Ramanathan, V., Kim, D., & Podgorny, I. A. (2005). Global anthropogenic aerosol direct forcing derived from satellite and ground-based observations. *Journal of Geophysical Research*, *110*(D24), D24207. https://doi.org/10.1029/2005JD006356
Forster, P. M., Richardson, T., Maycock, A. C., Smith, C. J., Samset, B. H., Myhre, G., et al. (2016). Recommendations for diagnosing effective radiative forcing from climate models for CMIP6. *Journal of Geophysical Research: Atmospheres*, *121*(20), 12460–412475. https://doi.org/10.1002/2016jd025320
Ghan, S. J. (2013). Estimating aerosol effects on cloud radiative forcing. *Atmospheric Chemistry and Physics*, *13*(19), 9971–9974. https://doi.org/10.5194/acp-13-9971-2013
Golaz, J.-C., Salzmann, M., Donner, L. J., Horowitz, L. W., Ming, Y., & Zhao, M. (2011). Sensitivity of the aerosol indirect effect to subgrid variability in the cloud parameterization of the GFDL atmosphere general circulation model AM3. *Journal of Climate*, *24*(13), 3145–3160. https://doi.org/10.1175/2010jcli3945.1
Goren, T., & Rosenfeld, D. (2014). Decomposing aerosol cloud radiative effects into cloud cover, liquid water path and Twomey components in marine stratocumulus. *Atmospheric Research*, *138*, 378–393. https://doi.org/10.1016/j.atmosres.2013.12.008
Hammer, M. S., van Donkelaar, A., Li, C., Lyapustin, A., Sayer, A. M., Hsu, C., et al. (2022). *Global Annual $PM_{2.5}$ Grids from MODIS, MISR and SeaWiFS Aerosol Optical Depth (AOD), 1998-2019, V4.GL.03*. NASA Socioeconomic Data and Applications Center (SEDAC).
Iacono, M. J., Delamere, J. S., Mlawer, E. J., Shephard, M. W., Clough, S. A., & Collins, W. D. (2008). Radiative forcing by long-lived greenhouse gases: Calculations with the AER radiative transfer models. *Journal of Geophysical Research*, *113*(D13), D13103. https://doi.org/10.1029/2008jd009944
Jia, H., Ma, X., Yu, F., & Quaas, J. (2021). Significant underestimation of radiative forcing by aerosol-cloud interactions derived from satellite-based methods. *Nature Communications*, *12*(1), 3649. https://doi.org/10.1038/s41467-021-23888-1
Jing, X., & Suzuki, K. (2018). The impact of process-based warm rain constraints on the aerosol indirect effect. *Geophysical Research Letters*, *45*(19), 10729–710737. https://doi.org/10.1029/2018gl079956
Kato, S., Rose, F. G., Rutan, D. A., Thorsen, T. J., Loeb, N. G., Doelling, D. R., et al. (2018). Surface irradiances of edition 4.0 Clouds and the Earth's Radiant Energy System (CERES) Energy Balanced and Filled (EBAF) data product. *Journal of Climate*, *31*(11), 4501–4527. https://doi.org/10.1175/jcli-d-17-0523.1
Khairoutdinov, M., & Kogan, Y. (2000). A new cloud physics parameterization in a large-eddy simulation model of marine stratocumulus. *Monthly Weather Review*, *128*(1), 229–243. https://doi.org/10.1175/1520-0493(2000)128<0229:ancppi>2.0.co;2
Liu, X., Easter, R. C., Ghan, S. J., Zaveri, R., Rasch, P., Shi, X., et al. (2012). Toward a minimal representation of aerosols in climate models: Description and evaluation in the Community Atmosphere Model CAM5. *Geoscientific Model Development*, *5*(3), 709–739. https://doi.org/10.5194/gmd-5-709-2012
Morrison, H., & Gettelman, A. (2008). A new two-moment bulk stratiform cloud microphysics scheme in the Community Atmosphere Model, version 3 (CAM3). Part I: Description and numerical tests. *Journal of Climate*, *21*(15), 3642–3659. https://doi.org/10.1175/2008jcli2105.1
Myhre, G., Shindell, D., Bréon, F.-M., Collins, W., Fuglestvedt, J., Huang, J., et al. (2013). Anthropogenic and natural radiative forcing. In T. F. Stocker, D. Qin, G.-K. Plattner, M. Tignor, S. K. Allen, J. Doschung, et al. (Eds.), *Climate change 2013: The physical science basis. Contribution of working group I to the fifth assessment report of the intergovernmental panel on climate change* (pp. 659–740). Cambridge University Press. https://doi.org/10.1017/CBO9781107415324.018
Na, Y., Fu, Q., & Kodama, C. (2020). Precipitation probability and its future changes from a global cloud-resolving model and CMIP6 simulations. *Journal of Geophysical Researcmh: Atmospheres*, *125*(5), e2019JD031926. https://doi.org/10.1029/2019jd031926
Neale, R. B., Richter, J. H., & Jochum, M. (2008). The impact of convection on ENSO: From a delayed oscillator to a series of events. *Journal of Climate*, *21*(22), 5904–5924. https://doi.org/10.1175/2008jcli2244.1
Park, S., Allen, R. J., & Lim, C.-H. (2020). A likely increase in fine particulate matter and premature mortality under future climate change. *Air Quality, Atmosphere & Health*, *13*(2), 143–151. https://doi.org/10.1007/s11869-019-00785-7
Park, S., & Bretherton, C. S. (2009). The University of Washington shallow convection and moist turbulence schemes and their impact on climate simulations with the Community Atmosphere Model. *Journal of Climate*, *22*(12), 3449–3469. https://doi.org/10.1175/2008jcli2557.1
Plant, R. S., & Craig, G. C. (2008). A stochastic parameterization for deep convection based on equilibrium statistics. *Journal of the Atmospheric Sciences*, *65*(1), 87–105. https://doi.org/10.1175/2007jas2263.1
PM2.5. (2022). PM2.5 concentrations [Dataset]. Retrieved from https://aqicn.org/data-platform/covid19
Rasch, P. J., Barth, M. C., Kiehl, J. T., Schwartz, S. E., & Benkovitz, C. M. (2000). A description of the global sulfur cycle and its controlling processes in the National Center for Atmospheric Research Community Climate Model, Version 3. *Journal of Geophysical Research*, *105*(D1), 1367–1385. https://doi.org/10.1029/1999jd900777
Roth, G. A., Abate, D., Abate, K. H., Abay, S. M., Abbafati, C., Abbasi, N., et al. (2018). Global, regional, and national age-sex-specific mortality for 282 causes of death in 195 countries and territories, 1980–2017: A systematic analysis for the Global Burden of Disease Study 2017. *The Lancet*, *392*(10159), 1736–1788.
Silva, R. A., West, J. J., Lamarque, J.-F., Shindell, D. T., Collins, W. J., Faluvegi, G., et al. (2017). Future global mortality from changes in air pollution attributable to climate change. *Nature Climate Change*, *7*(9), 647–651. https://doi.org/10.1038/nclimate3354
Slinn, W. G. N. (1984). Precipitation scavenging. In D. Randerson (Ed.), *Atmospheric Science and Power Production* (pp. 472–477). U.S. Department of Energy.
Smith, C. J., Kramer, R. J., Myhre, G., Alterskjær, K., Collins, W., Sima, A., et al. (2020). Effective radiative forcing and adjustments in CMIP6 models. *Atmospheric Chemistry and Physics*, *20*(16), 9591–9618. https://doi.org/10.5194/acp-20-9591-2020
Stochastic Convection Scheme. (2021). *Stochastic convection* [Software]. Zenodo. https://doi.org/10.5281/zenodo.4543261
Twomey, S. (1977). The influence of pollution on the shortwave albedo of clouds. *Journal of the Atmospheric Sciences*, *34*(7), 1149–1152. https://doi.org/10.1175/1520-0469(1977)034<1149:tiopot>2.0.co;2
Wang, X., Zhang, L., & Moran, M. (2010). Uncertainty assessment of current size-resolved parameterizations for below-cloud particle scavenging by rain. *Atmospheric Chemistry and Physics*, *10*(12), 5685–5705. https://doi.org/10.5194/acp-10-5685-2010

Wang, Y., Liu, X., Hoose, C., & Wang, B. (2014). Different contact angle distributions for heterogeneous ice nucleation in the Community Atmospheric Model version 5. *Atmospheric Chemistry and Physics*, *14*(19), 10411–10430. https://doi.org/10.5194/acp-14-10411-2014

Wang, Y., Xia, W., Liu, X., Xie, S., Lin, W., Tang, Q., et al. (2021). Disproportionate control on aerosol burden by light rain. *Nature Geoscience*, *14*(2), 72–76. https://doi.org/10.1038/s41561-020-00675-z

Wang, Y., & Zhang, G. J. (2016). Global climate impacts of stochastic deep convection parameterization in the NCAR CAM5. *Journal of Advances in Modeling Earth Systems*, *8*(4), 1641–1656. https://doi.org/10.1002/2016ms000756

Wang, Y., Zhang, G. J., & Craig, G. C. (2016). Stochastic convective parameterization improving the simulation of tropical precipitation variability in the NCAR CAM5. *Geophysical Research Letters*, *43*(12), 6612–6619. https://doi.org/10.1002/2016gl069818

Wang, Y., Zhang, G. J., & He, Y.-J. (2017). Simulation of precipitation extremes using a stochastic convective parameterization in the NCAR CAM5 under different resolutions. *Journal of Geophysical Research: Atmospheres*, *122*(23), 12875–812891. https://doi.org/10.1002/2017jd026901

Wang, Y., Zhang, G. J., Xie, S., Lin, W., Craig, G. C., Tang, Q., & Ma, H.-Y. (2021). Effects of coupling a stochastic convective parameterization with the Zhang–McFarlane scheme on precipitation simulation in the DOE E3SMv1. 0 atmosphere model. *Geoscientific Model Development*, *14*(3), 1575–1593. https://doi.org/10.5194/gmd-14-1575-2021

Xia, W., Wang, Y., & Wang, B. (2022). Decreasing dust over the Middle East partly caused by irrigation expansion. *Earth's Future*, *10*(1), e2021EF002252. https://doi.org/10.1029/2021EF002252

Xu, Y., & Lamarque, J. (2018). Isolating the meteorological impact of 21st century GHG warming on the removal and atmospheric loading of anthropogenic fine particulate matter pollution at global scale. *Earth's Future*, *6*(3), 428–440. https://doi.org/10.1002/2017ef000684

Zelinka, M. D., Andrews, T., Forster, P. M., & Taylor, K. E. (2014). Quantifying components of aerosol-cloud-radiation interactions in climate models. *Journal of Geophysical Research: Atmospheres*, *119*(12), 7599–7615. https://doi.org/10.1002/2014jd021710

Zhang, G. J., & McFarlane, N. A. (1995). Sensitivity of climate simulations to the parameterization of cumulus convection in the Canadian Climate Centre general circulation model. *Atmosphere-Ocean*, *33*(3), 407–446. https://doi.org/10.1080/07055900.1995.9649539

Zhao, H., Geng, G., Zhang, Q., Davis, S. J., Li, X., Liu, Y., et al. (2019). Inequality of household consumption and air pollution-related deaths in China. *Nature Communications*, *10*(1), 1–9. https://doi.org/10.1038/s41467-019-12254-x